J4J.7

THE USE OF SIMULATED RADAR REFLECTIVITY FIELDS IN THE DIAGNOSIS OF MESOSCALE PHENOMENA FROM HIGH-RESOLUTION WRF MODEL FORECASTS

Steven E. Koch[1], Brad Ferrier[2], Mark T. Stoelinga[3],
Ed Szoke[1,4], Steven J. Weiss[2], and John S. Kain[5,6]

[1] *NOAA Research – Forecast Systems Laboratory (FSL), Boulder, CO*
[2] *National Weather Service (NWS)/National Centers for Environmental Prediction (NCEP)*
[3] *University of Washington, Seattle, WA*
[4] *Cooperative Institute for Research in the Atmosphere (CIRA), Colorado State University, Ft. Collins, CO*
[5] *Cooperative Institute for Mesoscale Meteorological Studies (CIMMS)*
[6] *NOAA Research – National Severe Storms Laboratory (NSSL), Norman, OK*

1. INTRODUCTION

Composite radar reflectivity (the maximum reflectivity in the grid column) and single level radar reflectivity are becoming increasingly popular as a means for displaying forecast fields from high-resolution numerical weather prediction (NWP) models. Displays of composite equivalent radar reflectivity factor (hereafter, the "Reflectivity Product") have been produced from the output of NWP models for several years by modelers at the Center for Analysis and Prediction of Storms (CAPS), the National Center for Atmospheric Research (NCAR), and by the Local Analysis and Prediction (LAPS) group at the Forecast Systems Laboratory (FSL). This past winter, simulated radar reflectivity fields were produced over the entire CONUS domain during the Developmental Testbed Center (Bernardet et al. 2005) Winter Forecast Experiment (DWFE), and made available for experimental forecasting purposes to the National Weather Service (Koch et al. 2005). The fields were produced from 5-km Weather Research and Forecasting (WRF) model forecasts made by the NCAR Advanced Research WRF (ARW) model and the NCEP Nonhydrostatic Mesoscale Model (NMM). This past spring, model reflectivity fields from 2-km and 4-km versions of the ARW and a 4.5-km version of the WRF-NMM forecasts were utilized during the Storm Prediction Center - National Severe Storms Laboratory Spring Program (SPC/NSSL Spring Program; Kain et al. 2005). It has also recently become possible to compare the Reflectivity Product, as well as 1-km AGL reflectivity fields from models to high quality, three-dimensional, national radar reflectivity mosaic products on a 1-km Cartesian grid being developed at NSSL.

The Reflectivity Product offers major advantages over traditional precipitation forecast displays, including the obvious fact that radar reflectivity is easier to verify in real time by direct comparison with readily available, observed composite reflectivity products. In addition, there are subtler benefits of this product that are relevant to understanding mesoscale processes. The chief advantage of the model Reflectivity Product is that it allows one to more easily see detailed mesoscale and storm-scale structures capable of being forecast by finer resolution NWP models. Examples demonstrating this advantage for a variety of mesoscale phenomena are presented in this paper.

Before any meaning can be ascribed to the Reflectivity Product for the purpose of interpreting mesoscale model forecasts, it is important to understand how it is determined. The equivalent reflectivity factor is computed from the forecast mixing ratios of grid-resolved hydrometeor species, assuming Rayleigh scattering by spherical particles of known density and an exponential size distribution. During the DWFE, perceptible differences appeared in the general nature of the simulated reflectivity fields from the two WRF models for winter storms, most notably a greater coverage of reflectivity below ~25 dBZ in the case of the NMM compared to the ARW. On the other hand, for severe convective weather regions during the Spring Program, the NMM produced noticeably *lower* values of maximum reflectivity compared to the ARW versions, with the NMM values limited to less than ~50 dBZ. We explain how these differences are mostly attributable to the differences in model physics and postprocessing.

It is important to note that it is not possible to make a strict comparison between composite reflectivity computed from a model grid point and that measured by scanning radar. Since the radar resolution degrades with distance from the transmitter, scanning radars cannot detect hydrometeors in the lower atmosphere due to the earth's curvature effect, and numerous other considerations (ground clutter, anomalous propagation, bright bands…). Thus, any attempt to make direct comparisons between the model simulated reflectivity fields and radar measurements is replete with problems.

Corresponding author address: *Steven E. Koch, NOAA/OAR/FSL, R/FS1, 325 Broadway, Boulder, CO 80305-3328; e-mail <* Steven.Koch@noaa.gov*>*

2. DISPLAYS OF REFLECTIVITY PRODUCT AND ACCUMULATED PRECIPITATION: INFERRING MESOSCALE PROCESSES

The ARW and NMM versions of WRF run during DWFE and the SPC/NSSL Spring Program utilized different sets of physics. The ARW model used the WSM 5-class microphysics scheme, the YSU boundary layer scheme, the NOAH 5-layer land-surface model (LSM), and Dudhia shortwave and RRTM longwave radiation. The WRF-NMM model used the Ferrier microphysics scheme, MYJ 2.5 closure scheme for the boundary layer, a different version of the NOAH LSM, and the Lacis-Hansen shortwave and Fels-Schwartzkopf longwave schemes (all of which are used in the Eta model). No cumulus parameterization was invoked for either WRF model at grid spacing of 2, 4, 4.5, or 5 km. Each WRF model used the Eta / EDAS for boundary and initial conditions.

The Reflectivity Product was something new to look at for wintertime weather during DWFE, since it is not available from the operational models, nor had it been thoroughly examined during the winter in past NWP experiments performed at FSL, NCAR, or CAPS. The chief advantage of this product is that it allows one to more easily see the mesoscale structures forecast by fine resolution models, such as lake-effect snowbands, narrow cold-frontal rainbands, and various cloud structures in the marine boundary layer (Fig. 1) – structures that tend to get lost in accumulated precipitation fields. Propagating features tend to get smeared out by the temporal integration procedure (accumulation periods typically range from 1 – 3 h), especially for rain cells that propagate at a large angle with respect to the precipitation band axis.

There are many other situations where the Reflectivity Product is indispensable for readily visualizing mesoscale structures. The next example is of a dispersive gravity wave train ahead of a warm front associated with an occluding cyclone in the Midwest (Fig. 2). Five waves displaying values <20 dBZ are apparent in the Reflectivity Product field, but not in the 3-hourly accumulated precipitation field (hereafter referred to as the "Precipitation Product"). The waves appear to merge as they approach a confluence deformation zone on the western side of a pronounced ridge at 700 hPa (Fig. 2d), where a strong horizontal gradient in relative humidity is located. The gravity waves primarily affect the distribution of cloudiness ahead of the surface warm front in the middle and upper troposphere. This is a typical pre-warm frontal sequence of events, with wavelike (undulating) cirrostratus clouds preceding undulating altocumulus and nimbostratus. The NIDS composite radar mosaic display (Fig. 2c) hints at the presence of these forecast structures.

The third example demonstrating the added value of the Reflectivity Product is of multiple snowbands forecast for the 1 March 2005 New England snowstorm. Shown in Fig. 3 are the snowbands as seen in the Precipitation and Reflectivity Product fields from the ARW 5-km model for several times, and observed composite radar reflectivity fields (from the experimental NSSL product). The most coherent, long-lasting, and strongest of the snowbands was **A**, which propagated northward and then northwestward as the storm system developed off the East Coast. Bands **B** and **C** propagated transversely to the dominant southwesterly flow aloft. Band **D** was the most delineated of the bands; this transverse band formed later in the lifecycle of the storm. Thus, all but one of the four bands had a character consistent with gravity waves, similar in appearance to precipitation bands seen in other strong winter storms affecting this region (e.g., Bosart and Sanders 1986; Zhang et al. 2001). No significant temperature gradient supportive of either frontogenesis or conditional symmetric instability (CSI) was present in the vicinity of these bands (Koch et al. 2005). These bands are readily apparent in the Reflectivity Product displays, but are difficult to discern in the Precipitation Product (particularly for Bands **B** and **D**, and the enhanced reflectivity feature near the surface cold front on the border between Ohio and Pennsylvania).

The simulated reflectivity fields forecast by the ARW and NMM models are compared in Fig. 4. The NMM model displays a tendency to exhibit greater coverage of reflectivity < 25 dBZ. As proven below, this is the result of differences in the way liquid water and ice species are treated in the model microphysics schemes, principally the assumed size distributions for snow. Yet, the most striking feature is how similar the forecasts appear from the two WRF models, despite the fact that they use quite different numerics and physics schemes. In particular, the placement, orientation, and number of precipitation bands forecast by the two models are remarkably similar to one another. Comparison of these forecast band characteristics with the observed bands (Fig. 3) shows fairly good correspondence overall, particularly for bands **A** and **D**, though the details pertaining to the other two bands are only moderately well predicted (mainly the orientation of the bands).

Differences in the Reflectivity Product produced by the ARW and NMM models during the convective season exhibited quite a different behavior from that seen in DWFE. Reflectivity Product fields at 0300 and 0600 UTC 29 April 2005 in the Arkansas region forecast by the 4-km ARW, the 2-km ARW, and the 4-km WRF-NMM models are shown in Fig. 5. Differences in convection structure and coverage forecast by the models are unmistakable. The 2-km ARW model reflectivity display is most useful for diagnosing storm type. However, of particular significance are systematic differences in the area covered by reflectivity >45 dBZ between the ARW and WRF-NMM models exist: no values in excess of 50 dBZ are found for the NMM. This difference in the displays from the two models was also true for most other days during the Spring Program.

It is important to note that there were occasions – primarily during the cool season – when the strength and persistence of mesoscale phenomena were so pronounced that the precipitation forecasts were adequate in highlighting their existence. For example, Koch et al. (2005) present a case in which pronounced stationary bands in mean sea level pressure and precipitation fields were forecast by both WRF models to the north of the storm center during the severe New England blizzard of 23 January 2005. These bands were fixed to the terrain and the observations agreed with this prediction. The Reflectivity Product added little to the understanding of the underlying forcing by the terrain from what could be readily determined from the Precipitation Product in this case.

3. REFLECTIVITY PRODUCT DIFFERENCES BETWEEN THE WRF-NMM AND ARW

The following factors – roughly in decreasing order of importance – contribute to differences in posted radar reflectivities between the two WRF model systems:

a) The overall performance associated with the suite of physics packages and the complex interactions between physical parameterizations;
b) Differences in the treatment of various liquid water and ice species in the microphysics;
c) In the case of the ARW, different assumptions in the size distributions of precipitation between what is modeled in the ARW and what is assumed in the radar reflectivity calculations.

The differences in Reflectivity Product displays between the WRF-NMM and ARW models are chiefly attributable to the differences in physics packages, particularly the way various liquid water and ice species are treated in the model microphysics schemes. The WRF model estimates of simulated reflectivity values depend upon details of the model microphysical schemes employed in the NMM and ARW models. Both models use the $\sum(ND^6)$ method, in which N represents the number of spherical hydrometeors per unit size range per unit volume, D is the particle diameter, and the summation is over all diameters within the hydrometeor size distribution. Thus, the Rayleigh scattering assumption is made (small spherical hydrometeors whose diameter is much smaller than the radar wavelength). The "equivalent reflectivity" Z_e is actually computed, so as to allow for the existence of ice particles in the backscattered volume.

The WRF Single-Moment 5-class (**WSM5**) microphysics scheme used in the WRF-ARW model (Hong et al. 2004) treats the cloud condensate in the form of cloud water and cloud ice as a combined category, and precipitation in the form of rain and snow also as a combined category. The WRF-NMM uses the **Ferrier** microphysics scheme (Ferrier et al. 2002), which accounts for four classes of hydrometeors: suspended cloud liquid water, rain, a variable-density "large ice" category (snow, graupel, or sleet), and "small cloud ice" (suspended cloud ice with a fixed diameter). The WSM5 and Ferrier microphysics schemes are both single-moment schemes that assume Marshall–Palmer exponential size distributions for snow and rain. The most important difference between the two microphysical parameterizations concerns the assumptions for the size distributions for snow. As is proven immediately below, for the same snow mass content, differences in radar reflectivity will scale with differences in parameterized snow number concentrations between the two microphysical schemes.

a)

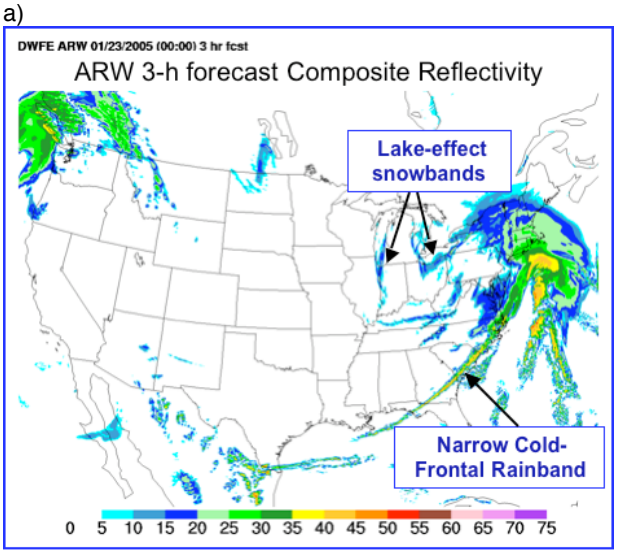

b)

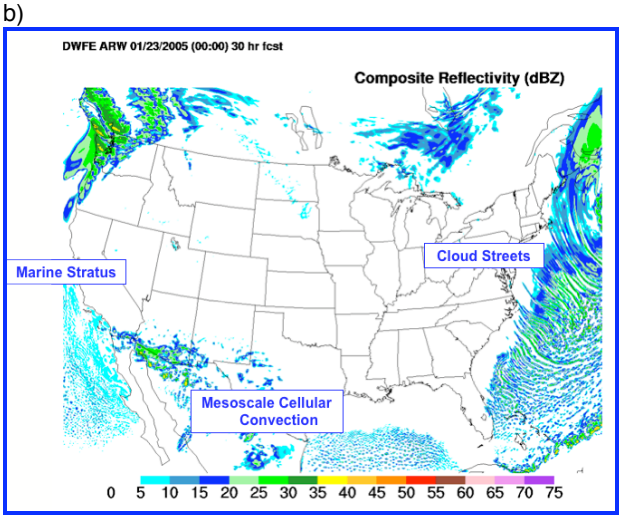

Fig. 1. Composite Reflectivity Product showing mesoscale phenomena forecast by the 5-km WRF models at a) 0300 UTC 23 January (3-h forecast) and b) 0600 UTC 24 January 2005 (30-h forecast). These boundary layer phenomena were not nearly as obvious in conventional precipitation forecast field displays (i.e., the accumulated precipitation product.

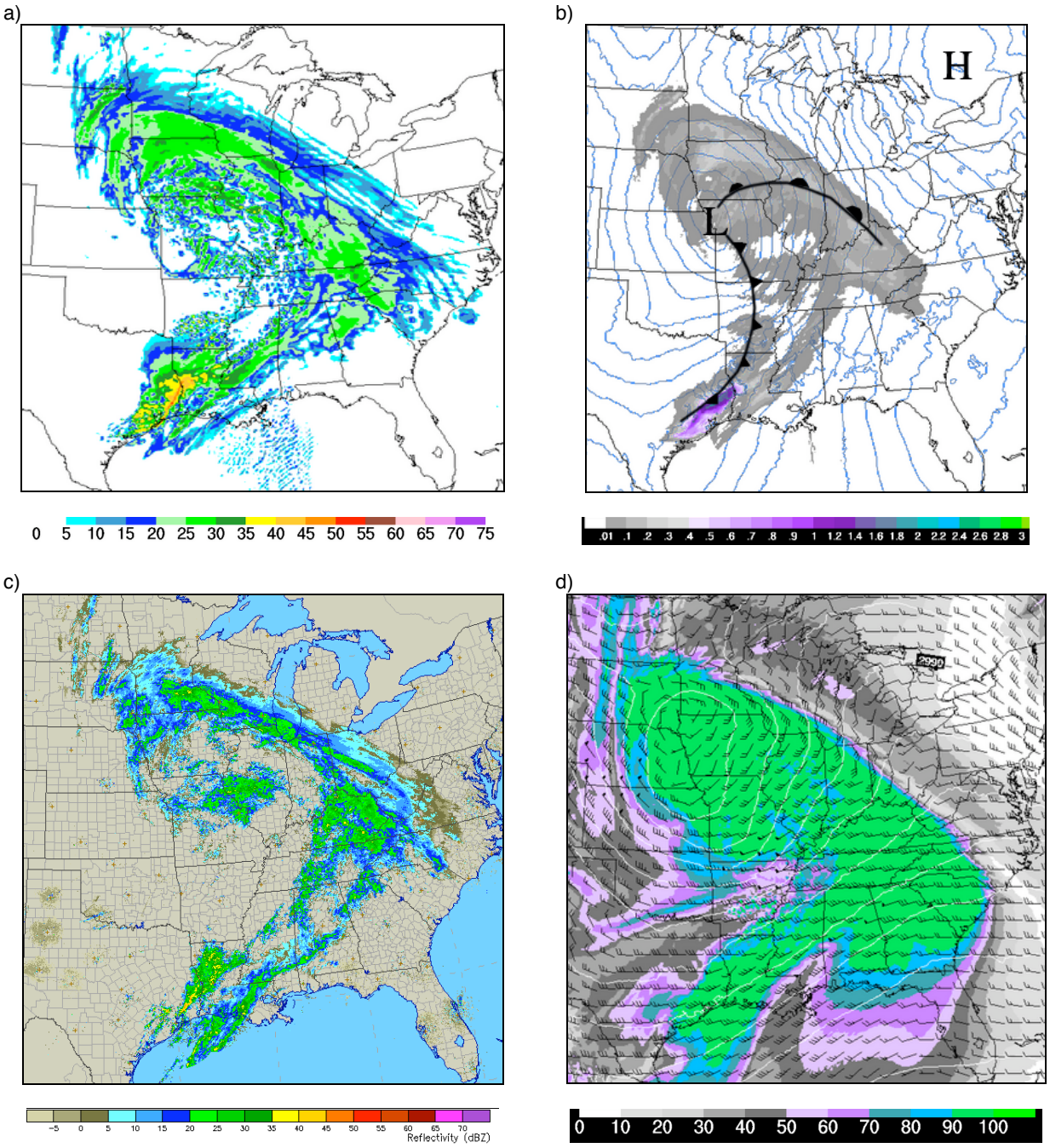

Fig. 2. Mesoscale bands in a cyclonic storm at 1800 UTC 13 February 2005: a) composite reflectivity field from 18-h ARW model forecast (dBZ, see colorbar), b) 3-hourly accumulated precipitation (inches, see colorbar) and MSLP field (1-hPa isobars), c) NIDS national analysis of composite reflectivity (dBZ, see colorbar), and d) winds (kt) and relative humidity (shaded) at 700 hPa.

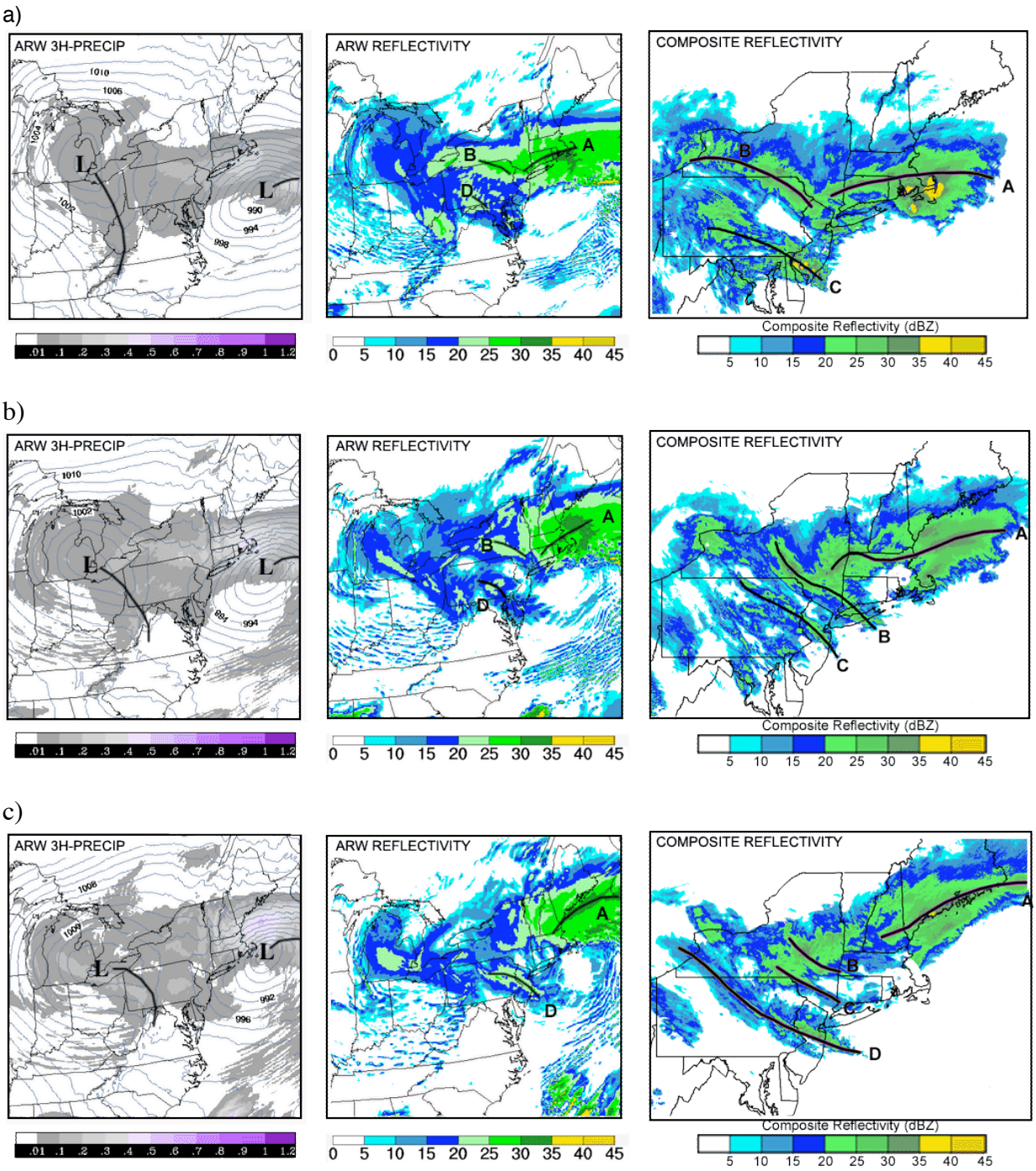

Fig. 3. Comparisons between appearance of snowbands A, B, C, and D seen in (left) 3-h accumulated precipitation fields from the ARW model, (middle) simulated composite radar reflectivity fields from the model forecasts, and (right) observed composite radar reflectivity fields for a) 3-h forecast verifying at 0300 UTC 1 March 2005, b) 6-h forecast verifying at 0600 UTC 1 March 2005, and c) 9-h forecast verifying at 0900 UTC 1 March 2005. Reflectivity factor displays from the model and observations use the same color scheme (dBZ). Mean sea level pressure (2 hPa isobar intervals) is superposed on the 3-hourly accumulated precipitation field (inches, see colorbar). Dark curves represent forecast surface cold front locations. Observed reflectivity field was obtained from experimental national mosaic product under development at the NOAA National Severe Storms Laboratory and adapted to have the same color scheme as used in the ARW Reflectivity Product.

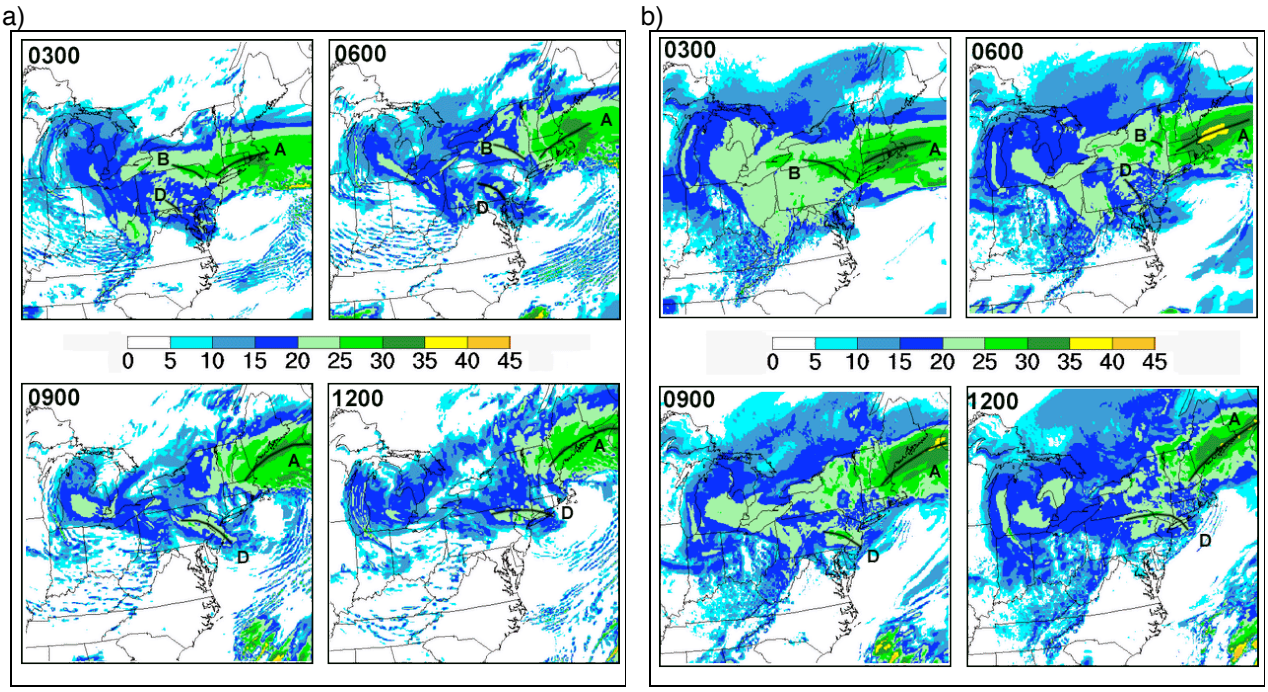

Fig.4. Simulated composite radar reflectivity fields (dBZ) at 0300, 0600, 0900, and 1200 UTC 01 March over the northeastern U.S. forecast by a) the ARW model, and b) the WRF-NMM model, showing precipitation bands. Note systematic differences in area covered by reflectivity < 25 dBZ between these two WRF models (considerably more for the NMM than for the ARW model).

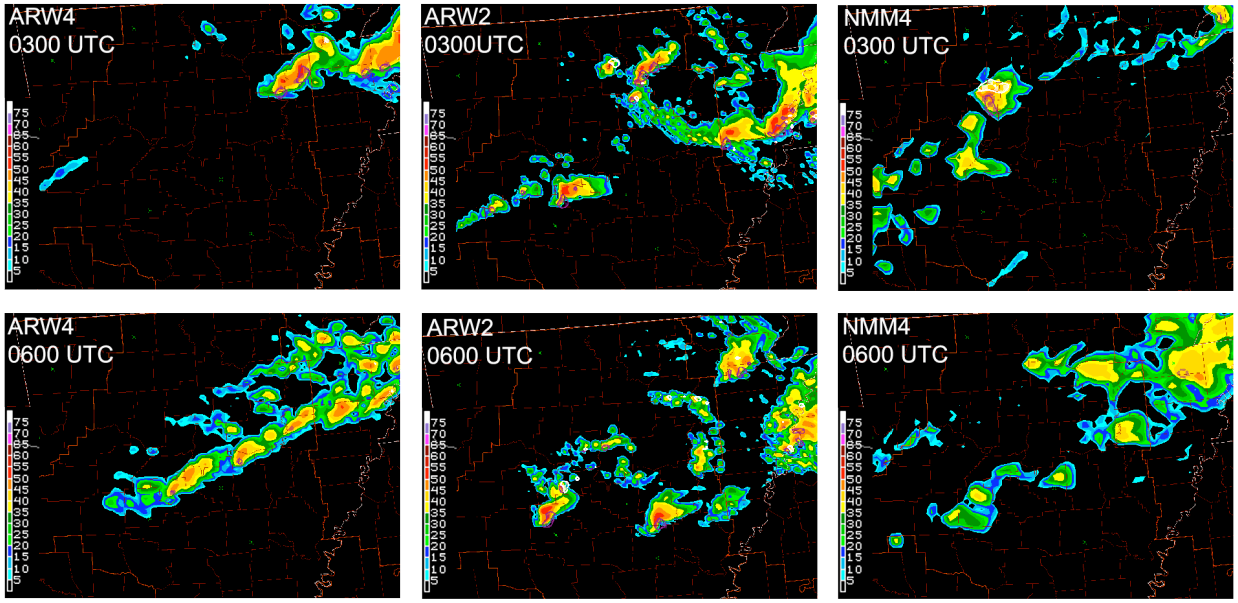

Fig.5. Simulated 1-km AGL radar reflectivity fields (dBZ) at 0300 and 0600 UTC 29 April 2005 in the Arkansas region as forecast by the ARW-4 km, the ARW-2 km, and the WRF-NMM-4 km models. While significant differences in forecast convection structure and coverage between the models are obvious, also note systematic differences in the area covered by reflectivity > 45 dBZ between the ARW and WRF-NMM models: no values in excess of 50 dBZ are found for the NMM (as was true for the other days in the Spring Program).

The exponential size distribution for snow assumed in both WSM5 and Ferrier is expressed as

$$\tilde{N}_s\left(D_S\right) = N_{0S}\exp\left(-\lambda_S D_S\right), \quad (1)$$

where $\tilde{N}_s\left(D_S\right)$ is the number of snow particles per unit size range per unit volume, N_{0S} is the snow intercept parameter, λ_S is the slope factor for snow, and D_S is the diameter of the frozen particles. The densities of raindrops, snow particles, and graupel particles are taken to be ρ_L =1000 kg m^{-3}, ρ_S = 100 kg m^{-3}, and ρ_G = 400 kg m^{-3}, respectively (ρ_L refers to the density of liquid water). All particles are assumed to be spheres of constant density. In order to obtain the expression for radar reflectivity for snow particles, we will first address the method for calculating equivalent reflectivity Z_e for raindrops. Assuming liquid water spheres and the Marshall–Palmer exponential size distributions, the sixth moment of the size distribution (equal to Z and Z_e for rain) is given as the equivalent reflectivity factor

$$Z_e = \Gamma\left(7\right)N_0\lambda^{-7}, \quad (2)$$

where Γ is the "gamma function," and $\Gamma(7)$ = 720. The slope factor λ can be obtained from the model-predicted rainwater mixing ratio q_{ra} and the density of dry air ρ_a as follows

$$\lambda = \left(\frac{\pi N_0 \rho_L}{\rho_a q_{ra}}\right)^{1/4}. \quad (3)$$

It is known that within the Rayleigh scattering regime, the radar cross section of an irregular ice particle is the same as a solid ice sphere of equivalent mass. While the assumed snow particles are spheres, they are not solid ice spheres. The diameter of the equivalent solid ice sphere is $D_{SOLID} = D_{SNOW}\left(\rho_S/\rho_I\right)^{1/3}$. Taking the sixth power of this relationship yields a factor of $\left(\rho_S/\rho_I\right)^2$ in the expression for equivalent reflectivity for the snow particles. Also, the reflective capacity of ice is less than that of water, by a factor equal to the ratio of the dielectric factor of ice $\left(\left|K\right|_I^2 = 0.176\right)$ to that of liquid water $\left(\left|K\right|_L^2 = 0.930\right)$, or 0.189. Considering these differences between ice and liquid water and the assumptions above, the equivalent reflectivity factor (2) for a population of snow particles can be written:

$$Z_e = 0.224\ \Gamma\left(7\right)N_0\lambda^{-7}\left(\frac{\rho_S}{\rho_I}\right)^2. \quad (4)$$

Since reflectivity, when not expressed in dBZ, is additive, the equivalent reflectivity value associated with each hydrometeor mixing ratio at a grid point can be calculated, and the values can be summed together to yield a total equivalent reflectivity factor. This quantity has MKS units of mm^6 m^{-3}, so Z_e should be multiplied by 10^{18} to convert it to radar dBZ units of mm^6 m^{-3}. The equivalent reflectivity in dBZ is then given by

$$Z_e \text{ (in dBZ)} = 10\log_{10}\left[Z_e \text{ (in mm}^6\text{ m}^{-3}\right], \quad (5)$$

The primary difference between the ARW and NMM displays of Z_e concerns the assumptions about the intercept parameter. For the WRF-ARW *output*, a constant, or "**fixed-intercept method**" was used during the DWFE and Spring Program, even though the WSM5 *model* microphysical scheme in the ARW model uses a temperature-dependent method for estimating N_0 ("**WSM5-consistent method**") as described by Thompson et al. (2004). In the fixed-intercept method, the intercept parameter N_0 is taken to be a constant value of 8x10^6, 2x10^7, and 4x10^6 m^{-4}, for rain, snow, and graupel, respectively. WSM5 and Ferrier both parameterize the snow intercept parameter as a function of the air temperature instead of assuming a constant:

$$N_{0S} = 2\times10^6\exp\left(-0.12T_c\right), \quad (6)$$

where T_c (°C) is the air temperature. The slope factor λ_S in the WRF-NMM output is specified in a manner consistent with the Ferrier microphysical scheme ("**Ferrier-consistent method**") as follows:

$$\lambda_s(mm^{-1}) = 1.0\exp(-.0536T_c). \quad (7)$$

This relation is based on airborne observations of precipitation ice spectra (Houze et al. 1979; Ryan 1996), which show that there is much less variability of λ_S with temperature than there is for N_{0S}. It is noted that for exponential particle size distributions, the mean diameter of snow $\bar{D}_S$ is equal to λ_S^{-1} (Ferrier assumes a value of $\bar{D}_S$ = 1 mm at 0°C).

The method used to compute the equivalent radar reflectivity factor for snow can be expressed in terms of total number concentration N_S instead of the intercept parameter N_{0S}, since for an exponential size distribution with mass concentration (or mixing ratio) predicted, specification of any one of the three quantities N, N_0, and λ_S uniquely determines the other two. Simple algebraic manipulation of (3), substitution of the equivalent expression $N_S = N_{0S}/\lambda_S$ for exponential functions, conversion to MKS units for radar (mm^6 m^{-3}) and some rearrangement leads to the following expression for the equivalent reflectivity factor:

$$Z_e = \left[\frac{(0.224)(720)\times 10^{18}}{(\pi\rho_L)^2}\right]\left(\frac{\rho_a q_S}{N_S}\right)^2$$

$$= 1.634\times 10^{13}\left(\frac{\rho_a q_S}{N_S}\right)^2 \qquad (8)$$

$$= 1.634\times 10^{4}\,\frac{M_S^2}{n_S}$$

where M_s is the snow mass content (g m^{-3}) and n_s is the snow number concentration per liter. A general derivation for gamma-distributed ice particle number concentrations, in which exponential distributions are a special subset, is also provided in Ferrier (1994). The implication of (8) is that, if the mass content and the number concentration of exponentially distributed ice hydrometeors are known, one can calculate the radar reflectivity. *Therefore, for the same mass content, differences in radar reflectivity will scale with differences in parameterized snow number concentrations between the various microphysical schemes*.

Assuming that the largest radar reflectivities due to snow from both forecast models most often occur at the 0ºC level and are associated with the largest particle sizes, then formulas describing equivalent radar reflectivity and total number concentration of snow valid at 0ºC can now be derived. Further manipulation of (3) results in the desired expression for the snow number concentration, upon inserting ρ_S = 100 kg m^{-3}, ρq_S = $10^3 M_S$, and N_S = 10^{-3} n_S (M_s in g m^{-3}, n_s in l^{-1}). The expressions for the fixed-intercept, the WSM5-consistent, and the Ferrier methods are, respectively:

$$(n_S)_{FI} = 12.63 M_S^{1/4} \qquad (9a)$$

$$(n_S)_{WC} = 2.246 M_S^{1/4} \qquad (9b)$$

$$(n_S)_{F} = 16.49 M_S \qquad (9c)$$

Finally, upon substituting equations (9) into (8), we obtain the expressions for the equivalent radar reflectivity factor for the three microphysics methods

$$(dBZ_{eS})_{FI} = 31.1 + 17.5\log M_S \qquad (10a)$$

$$(dBZ_{eS})_{FI} = 38.6 + 17.5\log M_S \qquad (10b)$$

$$(dBZ_{eS})_{FI} = 30.0 + 10\log M_S \qquad (10c)$$

Sample calculations for snow using these expressions show that Z_e = 13.6, 21.1 and 20.0 dBZ for the fixed-intercept, WSM5-consistent, and Ferrier-consistent methods, respectively, for a snow mass content of 0.1 g m^{-3}. Thus, the Ferrier-consistent method predicts 6.4 dBZ higher values than the fixed-intercept method used to display the Reflectivity Product for the ARW model at this snow mass content level. Relatively higher values for Ferrier occur for all mass contents smaller than 0.713 g m^{-3}. The difference between the Ferrier and WSM5 consistent methods is quite a bit smaller. Thus, it is not so much the difference in model microphysics that is important here, as much as it is the assumptions used in the model postprocessing to obtain the Reflectivity Product. This points out how easy it is to derive contradictory conclusions by calculating radar reflectivities that are not internally consistent with what is parameterized in the NWP model (i.e., the fixed-intercept method vs. the WSM5-consistent method).

The picture is quite a bit different, though, when convective storms with their typically high radar reflectivity values are considered. The NMM reflectivity values are considerably *lower* than those produced from the ARW as the result of the following assumptions made about the rain drop size distributions (DSDs) and precipitating ice (snow or graupel) spectra:

- The mean size of raindrops is assumed to be fixed at 0.45 mm for rain contents exceeding 1 g m^{-3}.
- The maximum number concentration of precipitating ice is assumed to be 20 per liter with a mean size of 1 mm at 0^{0}C, which corresponds to an effective intercept parameter of 2x10^7 m^{-4}.

These assumptions effectively limit the maximum reflectivity factor for the NMM to 52 dBZ, which is quite similar to what forecasters at SPC observed to be the case. However, there are other questions for which we do not yet have answers. It is unknown whether the higher reflectivities in the ARW may also manifest higher rain rates or greater snow and/or graupel contents, and for that matter, whether the dominant backscatter is from rain or ice as a function of the NWP model. Certainly the DSD assumptions can be changed, but the effects of doing so have not been determined not only for these reflectivity issues, but also, more importantly, for such concerns as the ability of the NMM to correctly produce the observed rain rates, which would be affected by evaporation and other processes that influence the DSD. While it would not be difficult to change the assumed particle spectra in the Ferrier microphysics scheme, it may make more sense to only change the methods used in the model postprocessor, where the reflectivity is actually calculated. These and other issues will be examined more thoroughly by scientists at the DTC and NCEP in the near future.

5. SUMMARY

In this paper, we have presented illustrations of the advantages to be gained by displaying the Reflectivity Product computed from NWP model forecast fields, in order to reveal the nature of mesoscale forcing and phenomena. During the cool season, the interactions between rainbands or snowbands and cloud features are made much easier to comprehend, and such phenomena as lake-effect snowbands, narrow cold-frontal rainbands, gravity waves, and so forth are readily revealed in the Reflectivity Product. During the warm season, convective storm structures (e.g., discrete cells,

lines, and multicell clusters) are more readily identified using reflectivity fields; in fact, when the grid spacing is decreased to 2 km, near storm-scale structures are apparent in the reflectivity fields. However, caution must be exercised in the proper interpretation of this product. We have shown that it can be very misleading to derive improper conclusions about the relative performance of different NWP models by calculating radar reflectivities that are not internally consistent with what is parameterized in the models. Mathematical analysis in this paper has revealed how the NMM and ARW versions of the WRF model may provide very different appearances for this product as the result of differences in assumptions made about the microphysics in the post-processing step. Issues remain about whether it is more appropriate to have full consistency between the microphysics in the NWP model and the reflectivity fields computed from the model postprocessor software, or whether it is preferable to employ one common method for computing reflectivity for all models.

During severe thunderstorm episodes in the 2005 Spring Program, forecasters also looked at 1-km AGL reflectivity, which avoided annoying ground-clutter signals that are more prevalent with composite reflectivity. Also, the model composite reflectivity field tended to substantially expand the coverage of low reflectivity regions, whereas the 1 km AGL reflectivity field more clearly indicated the existence of stronger convective storms in the model forecasts. Forecasters found it advantageous to focus on the 1 km AGL reflectivity fields for warm season deep convection, which could be easily compared to observed radar base reflectivity images. In the future, model hydrometeor and moisture fields also could be converted (using "forward models") into satellite radiance displays to help forecasters compare model output to satellite infrared (water vapor and window channel) imagery. Such operationally attractive and inventive fields, especially if produced at hourly intervals, are recommended.

6. ACKNOWLEDGMENTS

Nita Fullerton edited this paper to improve its readability. We wish to acknowledge the financial support for the DWFE obtained from the NWS/Office of Science and Technology (OST), the NOAA Office of Oceanic and Atmospheric Research (OAR), and the U.S. Weather Research Program (USWRP).

7. REFERENCES

Bosart, L.F., and F. Sanders, 1986: Mesoscale structure in the megalopolitan snowstorm of 11–12 February 1983. Part III: A large amplitude gravity wave. *J. Atmos. Sci.,* **43,** 924–939.

Bernardet, L.R., L.B. Nance, H.-Y. Chuang, A. Loughe, M. Demirtas, S. Koch, and R. Gall, 2005: The Developmental Testbed Center Winter Forecasting Experiment. *21st Conf. on Weather Analysis and Forecasting/17th Conf. on Numerical Weather Prediction*, Washington, D.C., Amer. Meteor. Soc.

Ferrier, B. S., 1994: A double-moment multiple-phase four-class bulk ice scheme. Part I: Description. J. Atmos. Sci., **51,** 249-280.

____, Y. Jin, Y. Lin, T. Black, E. Rogers, and G. DiMego, 2002: Implementation of a new grid-scale cloud and precipitation scheme in the NCEP Eta model. *15th Conf. on Numerical Weather Prediction*, San Antonio, TX, Amer. Meteor. Soc., 280-283.

Hong, S.-Y., H.-M. H. Huang, Q. Zhao, J. Dudhia, and S.-H. Chen, 2004: A revised approach to ice microphysical processes for the bulk parameterization of clouds and precipitation. *Mon. Wea. Rev.,* **132,** 103–120.

Houze, R.A., P.V. Hobbs, and P.H. Herzegh, 1979: Size distribution of precipitation particles in frontal clouds. *J. Atmos. Sci.,* **36,** 156–162

Kain, J.S., S.J. Weiss, M.E. Baldwin, G.W. Carbin, D.A. Bright, J.J. Levit, and J.A. Hart, 2005: Evaluating high-resolution configurations of the WRF model that are used to forecast severe convective weather: The 2005 SPC/NSSL Spring Program. *21st Conf. on Weather Analysis and Forecasting/17th Conf. on Numerical Weather Prediction*, Washington, D. C., Amer. Meteor. Soc., CD-ROM, 2A.5.

Koch, S.E., R. Gall, G. DiMego, E. Szoke, J. Waldstreicher, P. Manousos, B. Meisner, N. Seaman, M. Jackson, R. Graham, A. Edman, and D. Nietfeld, 2005: Lessons learned from the DTC Winter Forecast Experiment. *21st Conf. on Weather Analysis and Forecasting / 17th Conf. on Numerical Weather Prediction*, Washington, DC, Amer. Meteor. Soc.

Ryan, B.F., 1996: On the global variation of precipitating cloud layers. *Bull. Amer. Meteor. Soc.*, **77,** 53–70.

Thompson, G., R.M. Rasmussen, and K. Manning, 2004: Explicit forecasts of winter precipitation using an improved bulk microphysics scheme. Part I: Description and sensitivity analysis. *Mon. Wea. Rev.,* **132,** 519–542.

Zhang, F., S.E. Koch, C.A. Davis, and M.L. Kaplan, 2001: Wavelet analysis and the governing dynamics of a large-amplitude mesoscale gravity wave event along the East Coast of the United States. *Quart. J. Roy. Meteor. Soc.*, **127,** 2209–2245.